Swiss J Geosci (2013) 106:79–90
DOI 10.1007/s00015-013-0129-5

Earthquake focal mechanisms and stress orientations in the eastern Swiss Alps

Iris Marschall · Nicholas Deichmann · Federica Marone

Received: 16 July 2012 / Accepted: 26 April 2013 / Published online: 31 May 2013

Abstract This study presents an updated set of earthquake focal mechanisms in the Helvetic and Penninic/Austroalpine domains of the eastern Swiss Alps. In eight cases, based on high-precision relative hypocentre locations of events within individual earthquake sequences, it was possible to identify the active fault plane. Whereas the focal mechanisms in the Helvetic domain are mostly strike-slip, the Penninic/Austroalpine domain is dominated by normal-faulting mechanisms. Given this systematic difference in faulting style, an inversion for the stress field was performed separately for the two regions. The stress field in the Penninic/Austroalpine domain is characterized by extension oriented obliquely to the E–W strike of the orogen. Hence, the Penninic nappes, which were emplaced as large-scale compressional structures during the Alpine orogenesis, are now deforming in an extensional mode. This contrasts with the more compressional strike-slip regime in the Helvetic domain towards the northern Alpine front. Relative to the regional stress field seen in the northern Alpine foreland with a NNW–SSE compression and an ENE–WSW extension, the orientation of the least compressive stress in the Penninic/Austroalpine domain is rotated counter-clockwise by about 40°. Following earlier studies, the observed rotation of the orientation of the least compressive stress in the Penninic/Austroalpine region can be explained as the superposition of the regional stress field of the northern foreland and a uniaxial extensional stress perpendicular to the local trend of the Alpine mountain belt.

Keywords Switzerland · Seismotectonics · Stress inversion · High-precision hypocenter locations · Active faulting

Editorial handling: Ann Hirt and A. G. Milnes.

Electronic supplementary material The online version of this article (doi:10.1007/s00015-013-0129-5) contains supplementary material, which is available to authorized users.

I. Marschall · N. Deichmann (✉) · F. Marone
Swiss Seismological Service, ETH Zurich, Sonneggstrasse 5, 8092 Zurich, Switzerland
e-mail: deichmann@sed.ethz.ch

Present Address:
F. Marone
Paul Scherrer Institute, 5232 Villigen, Switzerland

1 Introduction

The analysis of earthquake focal mechanisms to derive information about the style of deformation and the state of stress in the brittle layers of the Earth's crust is a well-established procedure. This information constitutes a substantial contribution to our understanding of the current tectonics of a given region. In addition, the slope of earthquake recurrence relations (the so-called b-value of the empirical Gutenberg-Richter law), which determines the relative frequency of occurrence of large and small earthquakes, differs for different stress regimes (Schorlemmer et al. 2005). Thus, observations of regional differences in the state of stress are important input for the definition of source zones used in seismic hazard assessments.

The first comprehensive seismotectonic map of Switzerland, published by Pavoni and Mayer-Rosa (1978), showed that the then available focal mechanisms in the Swiss Alps and northern Alpine foreland were compatible with a crust deforming as a consequence of the ongoing convergence between Europe and Africa and of spreading along the northern Atlantic ridge. As more focal-mechanism data became available, this picture was gradually refined. A

detailed analysis of focal mechanisms in the Valais (Eva et al. 1998) and a microseismic study with a temporary network of portable seismographs (Maurer et al. 1997) revealed striking differences between the deformation observed in the Helvetic domain north of the Rhone valley and the Penninic domain to the south. Seismicity in the Helvetic nappes and the underlying basement is characterized mainly by strike-slip events, compatible with the expected crustal shortening. In the Penninic nappes, which formed earlier in the Alpine orogeny as a consequence of large-scale thrusting, present-day earthquake focal mechanisms are evidence of extensional deformation oriented obliquely to the general E–W trend of the mountain range. Stress inversions of earthquake focal mechanisms in the Valais confirmed this difference (Maurer et al. 1997; Kastrup 2002; Kastrup et al. 2004). Similar differences in style of deformation and state of stress have been observed also in the Western Alps of France and Italy (Eva et al. 1997; Eva and Solarino 1998; Sue et al. 1999; Delacou et al. 2004).

The results of a 2-year microseismic study with a temporary network of portable seismographs in Graubünden and the upper reaches of the Rhine Valley of St. Gallen suggested that there are substantial differences in faulting style between the Helvetic domain of eastern Switzerland and the Penninic/Austroalpine domain (Roth et al. 1992; Pavoni et al. 1997). These differences have also been noted by Persaud and Pfiffner (2004) in a comparison of post-glacial faults and lineaments with earthquake focal mechanisms in the eastern Swiss Alps.

In a large-scale study of deformation and stress in the Western and Central Alps, Delacou et al. (2004) included also the eastern Swiss Alps in their stress inversion. However, as noted by Kastrup et al. (2004), it is questionable whether the focal mechanism data available at that time were sufficient to perform a well-constrained stress inversion for that region. So the question whether a similar change in stress regime and orientation as in the western Swiss Alps exists also in the east remained to be answered. Meanwhile, the number of events for which focal mechanisms could be derived increased substantially. In this article we present the results of a stress inversion based on all focal mechanisms available to date in the eastern Swiss Alps. A detailed documentation of the eight earthquake sequences for which it was possible to identify the active fault plane can be found in the Appendix, which is included as an electronic supplement (online resource 1).

2 Tectonic setting and seismicity

The region of interest in this study comprises four major tectonic units: the Helvetic domain at the northern Alpine front, the Aar- and Gotthard-crystalline massifs, the complex stack of Penninic nappes in the southwest and the Austroalpine domain to the east and southeast (Fig. 1). The Helvetic domain consists mainly of Mesozoic sedimentary nappes overlying the Tertiary sediments of the Alpine foreland in the north and the Variscan crystalline basement further south. The latter manifests itself in the Aar–Gotthard massif, exposed to the west of our profile (Fig. 1). The Penninic nappes form a complex sequence of nappes consisting of both sedimentary and crystalline units that have been piled up during the earlier thrusting episodes of the Alpine orogeny. As illustrated by the cross-section in Fig. 2, these two structural elements—the Helvetic nappes (including the underlying Infrahelvetic units and the Aar and Gotthard basement) and the Penninic nappes—are the dominant tectonic features in the western part of the region of interest. Further to the east, the region is characterized by the remains of both sedimentary and crystalline Austroalpine units that cover the underlying Penninic nappes. More detailed discussions of the structure of the eastern Swiss Alps can be found in Pfiffner and Hitz (1997) and in Schmid et al. (1997).

In Fig. 3, we show the epicentres of the earthquakes with magnitudes $M_L \geq 2$ recorded between 1984 and 2012 in Switzerland and surroundings. During this period, the seismic activity in the region of interest was largest in the east and south-east, comprising parts of both the Helvetic and Penninic/Austroalpine domains, where the earthquakes tended to occur in pronounced clusters. In the western part of the study area, which comprises parts of the Penninic domain and the adjacent Aar–Gotthard region, the recent seismic activity has been comparatively low. As already noted by Roth et al. (1992) and confirmed by all subsequent observations, focal depths below the eastern Swiss Alps are restricted to the upper 10–15 km of the crust. In the cross-section shown in Fig. 2, we have plotted the hypocentres of those events for which we have focal mechanisms and which lie within a horizontal distance of 12 km from the profile. This shows that, in the Helvetic domain, many of the significant events occurred within the sedimentary units below the Helvetic nappes or within the immediately underlying basement. Further to the south, the hypocentres are located in the stack of the Penninic nappes.

3 Focal mechanisms

The set of focal mechanisms available for the present study comprises a total of 44 events (28 in the Helvetic domain and 16 in the Penninic/Austroalpine domain). The corresponding parameters are listed in Table 1, and the fault-plane solutions are plotted on the tectonic map in Fig. 4. Thus, the available data set has more than doubled compared to that available to Kastrup et al. (2004) and to Delacou et al. (2004). The magnitudes (M_L) of these events

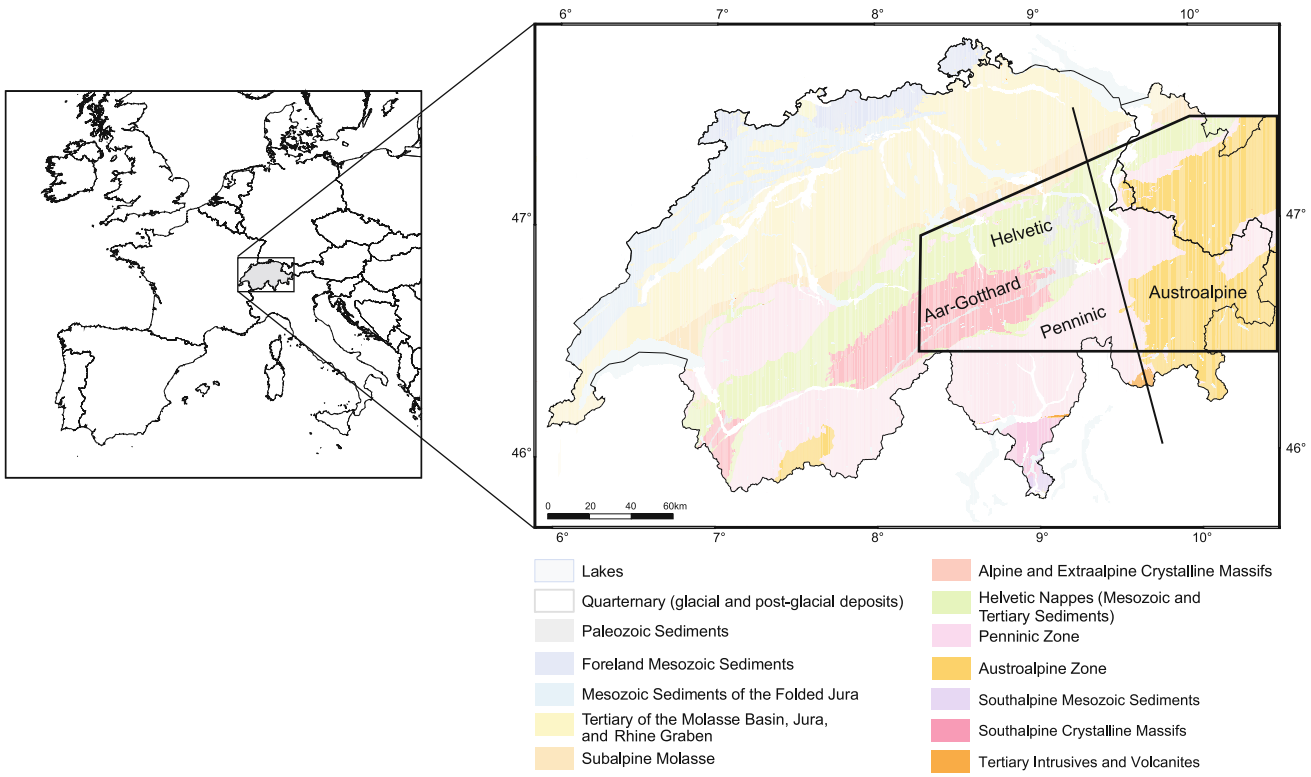

Fig. 1 Europe with Switzerland (*left*) and a tectonic map of Switzerland (*right*) showing the major tectonic elements (Bundesamt für Wasser und Geologie 2005). The study area is outlined by the *trapezoidal frame*, and the *oblique line* is the trace of the cross-section in Fig. 2

range between 2.1 and 5.0, and computed focal depths range from 1 to 11 km, with an average depth of about 5 km. As discussed in more detail in the Appendix (online resource 1) and in the various other references to the corresponding focal mechanisms, the typical focal-depth uncertainty is on the order of 3 km.

For the two events of Buchs (H9) and Quinten (H13) focal mechanisms are computed from full-waveform moment-tensor inversions (see Braunmiller et al. 2002 for an overview of the method). Focal mechanisms of the two Bormio events (P7 and P9) are taken from a still ongoing study of the sequence that these events are part of, and their parameters are very similar to results of the full-waveform moment-tensor inversions of Braunmiller et al. (2002). All other focal mechanisms are derived from fault-plane solutions based on first-motion polarities, either published previously in the literature (see Table 1 for references) or documented in the Appendix (online resource 1). In order not to give undue weight to earthquake sequences with several essentially identical events, only one mechanism, generally of the strongest event in the sequence, is listed in Table 1 and is used for the stress inversion. For sequences with several focal mechanisms that differ significantly from each other, Vaz (P5 and P6), Bormio (P7 and P9), Wildhaus (H24, H25 and H27), we selected those events whose mechanisms are well constrained and which are representative of the observed variability. In the case of the Vaz sequence, event P6 was chosen because, as documented in the Appendix (online resource 1), for this event it was possible to identify the active fault plane.

The preponderance of strike-slip mechanisms and some thrust events in the Helvetic domain, in contrast to the normal faulting events that dominate in the Austroalpine and Penninic domain, is clearly visible in Fig. 4. As listed in Table 1, we have therefore subdivided the data set according to their tectonic setting. For some of the events located in the border region between tectonic units, it might be debatable to which domain they should be attributed. This applies in particular to the events of Bad Ragaz (event numbers H15 and H21) as well as to the events of Vaduz (H26) and Feldkirch (H28). Given that the surface extent of the different tectonic units is the expression of processes that occurred in the distant past and that the focal mechanisms of the events recorded over the last 30 years represent the present stress field, we separated the two data subsets according to their geographical location rather than by following strictly the tectonic boundaries.

The difference in faulting style between the Helvetic and the Penninic/Austroalpine domains is illustrated also by the stereographic projections of the P- and T-axes in Fig. 5. In the Helvetic domain, the P-axes are nearly all more or less horizontal, with two exceptions that

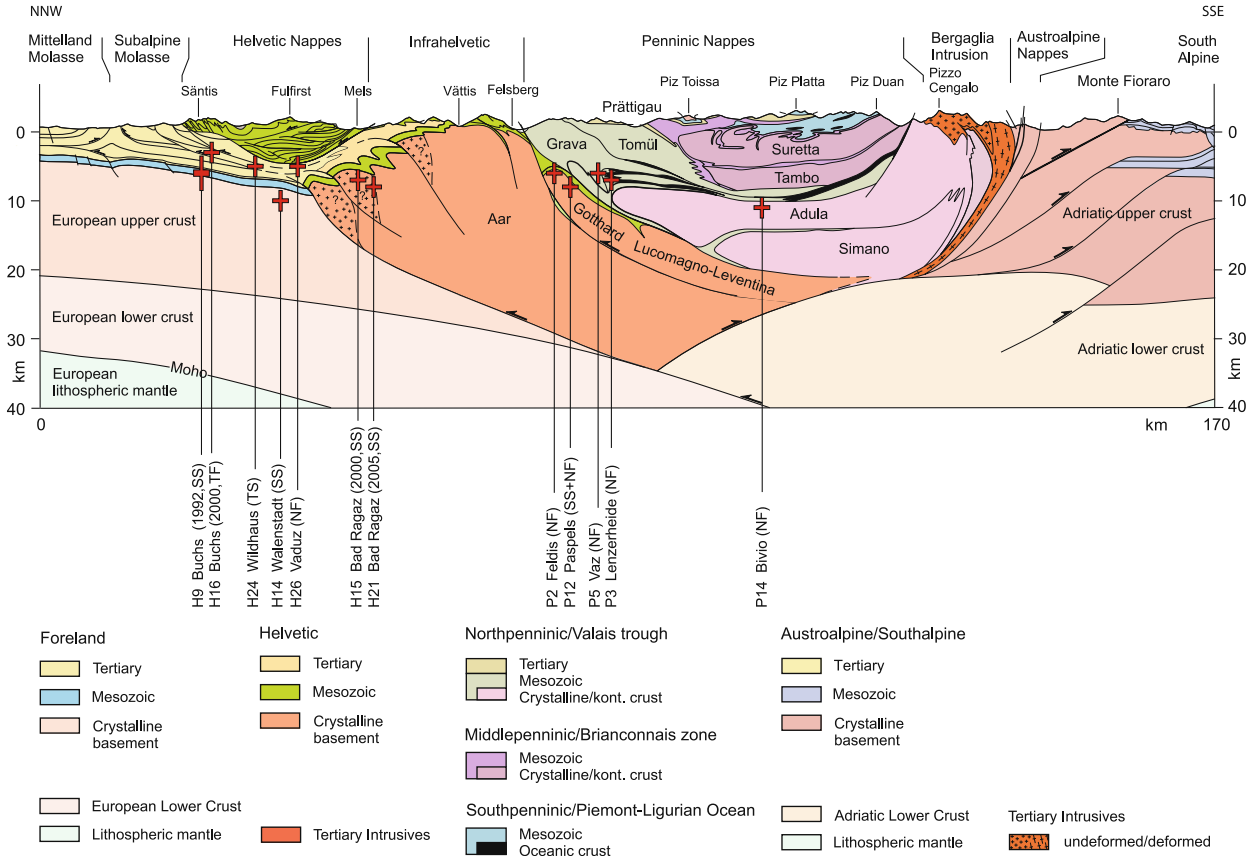

Fig. 2 Tectonic cross-section across the eastern Swiss Alps, modified after Nagra (2008), based on Pfiffner et al. (1997) and references therein. The *red crosses* denote the hypocentres of earthquakes with focal mechanisms, located within a maximum distance of 12 km to the trace of the cross-section (for the three Wildhaus events only one *symbol is plotted*). *SS* strike-slip fault, *NF* normal fault, *TF* thrust fault, *TS* thrust fault with strike slip component

correspond to the normal faulting mechanism of Sachseln and Vaduz (event numbers H2 and H26 in Table 1; Fig. 4), while the variability of the plunge of the T-axes is typical of a strike-slip regime with some thrust faults. In the Penninic/Austroalpine domain, all the T-axes lie close to horizontal, while the plunge of more than half of the P-axes is steep, typical of a normal faulting environment with some strike-slip events. Note however, that the average azimuthal orientation of the axes does not seem to differ by more than 10° between the two domains. Figure 5 shows also the orientation of the nodal planes in a polar histogram (rose diagram) and the orientation of the poles of the nodal planes in a stereoplot separately for the two tectonic regions. For the sake of consistency, these diagrams include both nodal planes also for those ten events for which we were able to identify the active fault plane (see chapter 4 and online resource 1). In the Penninic/Austroalpine domain, most nodal planes tend to bundle more closely along a direction perpendicular to the mean orientation of the T-axes, as is to be expected for a normal faulting environment, while in the Helvetic domain most nodal planes tend to form two sets more or less perpendicular to each other in accord with a strike-slip environment. At least qualitatively, the observed variability in faulting style confirms the conceptual model proposed by Roth et al. (1992), based on a much smaller data set.

4 Stress inversion

The fundamental assumption underlying all methods to derive information about the stress field from focal mechanisms is that this field is homogeneous over the entire region under consideration. Obviously, the difference in faulting style observed across the eastern Swiss Alps contradicts this assumption for the region as a whole. Hence, the stress inversion must be performed separately for the Penninic/Austroalpine domain and for the Helvetic domain (Table 1). In addition, based on the results of the stress inversion discussed below, we tested the stress-homogeneity of the Helvetic domain, by performing the inversion on an eastern and a western subset of the Helvetic data separately (the eastern subset is taken from the smaller region outlined in Fig. 4).

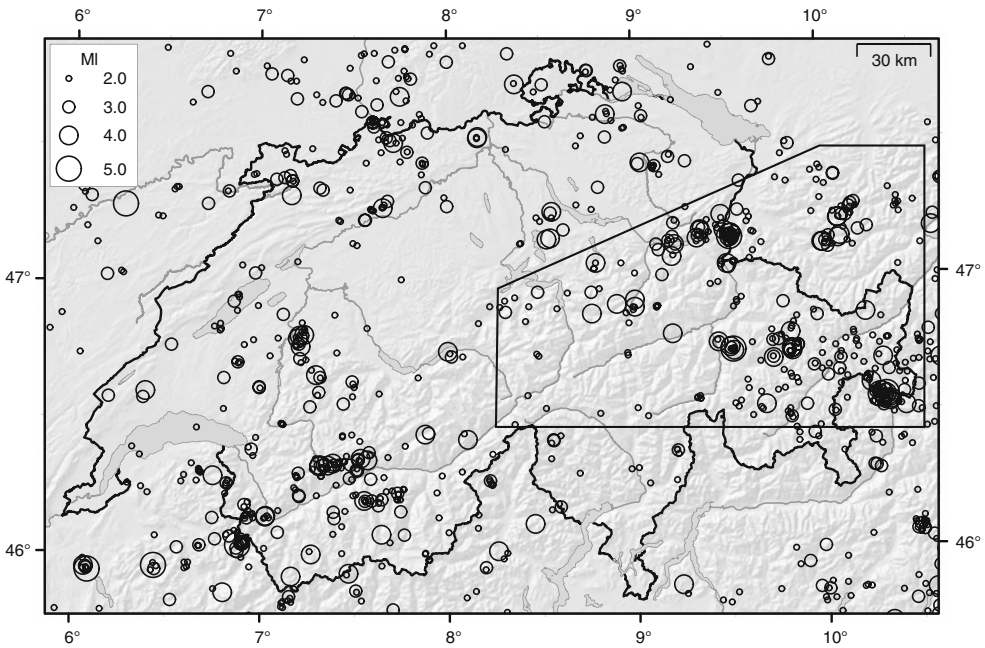

Fig. 3 Map of earthquake epicentres in Switzerland and surroundings for the time period of January 1984–February 2012 ($M_L \geq 2.0$). The study area is outlined by the *trapezoidal frame*

The quality of stress inversions based on focal mechanisms can be improved if the fault on which the earthquake actually occurred can be identified. However, from a fault-plane solution it is not possible to decide which of the two nodal planes corresponds to the active fault. In some cases, the analyzed events are part of a cluster of earthquakes with similar signals and the same focal mechanism. High-precision relative-location techniques, based on arrival-time differences determined from signal correlations, show that the hypocentres of individual events in such clusters usually lie on a plane that matches one of the nodal planes of the focal mechanism. In the Appendix to this article (online resource 1) we document the previously unpublished results of such relative hypocentre locations for eight earthquake clusters, whose focal mechanisms are part of the data set used for our stress inversion (see the Electronic Supplement). Together with the events of Steinibach and Oberrickenbach analyzed by Roth et al. (1992) and Deichmann et al. (2000) we can thus identify the active fault-plane in a total of eleven cases. Unfortunately, only the Paspels sequence of 2007–2009 is located in the immediate vicinity of recent-tectonic faults as mapped by Persaud and Pfiffner (2004), but in this case the active fault plane at depth strikes E–W, whereas the faults mapped at the surface nearest to the epicentre strike more or less N–S. Nevertheless, the E–W striking fault plane of the Paspels sequence is in accord with a prominent series of recently active E–W striking faults mapped along a band extending from the Vorab region in the west all the way to Klosters in the east (Fig. 11 of Persaud and Pfiffner 2004). However, as noted by Persaud and Pfiffner (2004), it is unlikely that any of the recently activated faults that they mapped are direct surface expressions of earthquake faults at depth, but that they are at best secondary features related to such earthquakes.

The method we used for the stress inversion is a linear inversion method introduced by Michael (1984, 1987a). The objective of this method is to minimize the angle between the direction of slip and the direction of the maximum shear stress resolved onto the fault while keeping strike and dip of fault plane fixed. Input data for the stress inversion are dip direction, dip angle and rake, for each earthquake focal mechanism. To address the problem of the ambiguity of not knowing the active fault plane, Michael (1987a, b) applied a bootstrapping method. This leaves all possible fault planes (active and auxiliary planes) in the data set so that they can be chosen randomly during the stress inversion computation. In our data set, some active fault planes are known. For each of these cases, the active fault plane is taken twice while excluding the other one, thereby giving it a larger weight in the inversion. The results of the inversion are trend and plunge of the three principal axes of the stress tensor as well as the ratio of the differences between the magnitudes of the three stress axes defined as $\Phi = (S2-S3)/(S1-S3)$, with $S1 > S2 > S3$. An alternative definition of the ratio of differential stresses is $R = (S2-S1)/(S3-S1)$, as given in Kastrup et al. (2004). The two definitions are equivalent and are related through $R = 1-\Phi$. The optimum orientations of the stress axes are shown together with their scatter as derived from the bootstrap analysis in the stereo-plots in Fig. 6, and the corresponding parameters are listed in Table 2, together with the value and standard deviation of Φ and of the angle β. The latter is the average misfit between the observed slip

Table 1 Focal mechanism parameters

Nr.	Location	Date	Lat./long.	z (km)	Ml	Nodal plane1 strike/dip/rake	Nodal plane2 strike/dip/rake	P-axis	T-axis	Type
Helvetic										
H1	Kerns	29.09.1985	46.922/8.308	1	2.5	39/26/122	184/68/75	285/22	70/64	TF
H2	Sachseln	21.12.1985	46.880/8.311	2	2.9	320/46/−63	104/50/−115	307/71	211/02	NF
H3	Steinibach	26.07.1987	46.890/9.121	1	2.4	**90/72/144**	193/56/22	145/10	47/38	SS
H4	Mürtschen	28.10.1987	47.078/9.196	7	4.2	178/70/13	84/78/160	132/05	40/23	SS
H5	Feldkirch	01.11.1987	47.225/9.617	1	2.6	295/78/−169	203/79/−12	159/16	249/01	SS
H6	Weesen	02.04.1989	47.144/9.111	8	3.2	31/43/87	215/47/93	303/02	168/87	TF
H7	Engelberg	19.11.1989	46.845/8.416	6	2.4	196/45/08	100/84/135	157/25	47/35	UD
H8	Linthal/Tödi	22.11.1990	46.890/8.999	5	3.6	341/60/06	248/85/150	298/17	200/24	SS
H9	Buchs	08.05.1992	47.266/9.498	6	4.6	102/63/−160	03/72/−28	321/32	54/06	SS
H10	Schächental	28.08.1994	46.875/8.777	4	3.9	68/56/156	172/70/36	297/09	34/39	SS
H11	Iberg	16.11.1995	47.057/8.798	4	3.8	16/45/00	286/90/135	341/30	231/30	UD
H12	Oberrickenbach	07.12.1996	46.913/8.425	2	2.5	**172/74/36**	70/56/160	297/11	36/37	SS
H13	Quinten	22.11.1997	47.134/9.189	1	3.8	256/28/83	84/62/94	171/17	04/73	TF
H14	Walenstadt	21.04.1998	47.140/9.338	10	3.6	209/78/06	118/84/168	164/04	73/13	SS
H15	Bad Ragaz	23.02.2000	47.052/9.499	7	3.6	**183/56/18**	83/75/145	137/12	38/35	SS
H16	Buchs	04.03.2000	47.250/9.470	3	3.6	235/20/90	55/70/90	145/25	325/65	TF
H17	Beckenried	17.08.2000	46.954/8.480	10	3.0	280/80/172	11/82/10	145/01	235/13	SS
H18	Linthal	17.03.2001	46.912/9.009	3	3.8	82/80/175	173/85/10	307/03	38/11	SS
H19	Urnerboden	06.05.2003	46.905/8.908	3	4.0	264/74/−169	171/79/−16	127/19	218/03	SS
H20	Nesslau	01.10.2003	47.200/9.216	8	3.0	102/78/−172	10/82/−12	326/14	57/03	SS
H21	Bad Ragaz	27.05.2005	47.034/9.509	8	2.9	189/75/19	94/72/164	321/02	52/24	SS
H22	Muotathal	12.07.2007	46.949/8.771	2	3.0	76/82/−178	346/88/−8	301/07	31/04	SS
H23	Ilanz	09.11.2008	46.793/9.212	8	3.7	163/58/−01	254/89/−148	123/23	24/21	UD
H24	Wildhaus	04.01.2009	47.173/9.361	5	4.1	99/54/155	204/70/39	328/10	67/41	TS
H25	Wildhaus	04.01.2009	47.176/9.375	5	3.1	**124/85/175**	214/85/05	349/00	79/07	SS
H26	Vaduz	17.01.2009	47.139/9.529	5	3.0	**329/66/−72**	110/30/−125	270/64	45/19	NF
H27	Wildhaus	12.08.2009	47.181/9.354	4	2.9	**291/89/179**	21/89/01	156/00	246/01	SS
H28	Feldkirch	25.10.2010	47.243/9.564	5	3.0	250/60/108	37/35/62	327/13	198/69	TF
Penninic/Austroalpine										
P1	St. Moritz	29.04.1987	46.493/9.821	8	2.6	353/67/−12	88/79/−156	312/24	219/08	SS
P2	Feldis	17.04.1988	46.783/9.467	6	2.2	327/43/−59	108/54/−115	321/69	216/06	NF
P3	Lenzerheide	23.05.1988	46.726/9.642	7	2.1	345/47/−54	118/54/−122	328/64	230/04	NF
P4	Davos	18.03.1990	46.792/9.837	4	3.5	326/38/−38	88/68/−121	317/56	201/17	NF
P5	Vaz	20.11.1991	46.731/9.527	6	5.0	294/37/−72	92/55/−103	321/76	191/09	NF
P6	Vaz	29.03.1992	46.736/9.513	7	2.8	**312/54/−83**	120/37/−100	253/80	37/08	NF
P7	Bormio	29.12.1999	46.530/10.250	6	4.9	345/45/−80	151/46/−100	341/83	248/00	NF
P8	Klosters	22.02.2000	46.854/9.994	4	3.3	174/68/−10	268/81/−158	133/22	39/09	SS
P9	Bormio	01.10.2001	46.559/10.304	6	4.1	304/45/−120	163/52/−63	135/69	235/04	NF
P10	Sertig	18.07.2003	46.723/9.831	7	3.9	105/44/−127	331/56/−60	296/64	40/07	NF
P11	Val Mora	12.04.2006	46.597/10.259	2	3.5	293/32/−130	158/66/−68	103/62	232/18	NF
P12	Paspels	21.01.2008	46.760/9.451	8	4.0	**87/81/−127**	345/38/−15	322/42	205/27	UD
P13	La Stretta	13.12.2008	46.498/10.059	2	3.2	**169/80/−3**	260/87/−170	125/09	34/05	SS
P14	Bivio	11.09.2009	46.527/9.696	11	3.6	**104/53/−115**	322/44/−61	315/70	211/05	NF
P15	Scalettapass	03.12.2011	46.666/9.955	9	2.8	291/42/−120	149/55/−66	114/69	222/07	NF

Table 1 continued

Nr.	Location	Date	Lat./long.	z (km)	Ml	Nodal plane1 strike/dip/rake	Nodal plane2 strike/dip/rake	P-axis	T-axis	Type
P16	Filisur	02.01.2012	46.700/9.737	6	3.5	**130/37/−103**	327/54/−80	274/78	50/08	NF

Strike, dip and rake of the nodal planes follow the convention of Aki and Richards (1980), where the plane dips to the right when viewed in the direction of strike. The parameters of the P- and T-axes are given as azimuth and plunge. In bold are those nodal planes that have been identified as the active fault planes. Type specifies the faulting type according to the classification of Zoback (1992): *SS* strike-slip fault, *NF* normal fault, *TF* thrust fault, *TS* oblique thrust fault, *NS* oblique normal fault, *UD* undefined. References: online resource 1 (Appendix), H15, H24–27, P5–6, P12–14, P16; Baer et al. (1999), H14; Baer et al. (2001), H16–17, P8; Baer et al. (2007), P11; Bernardi et al. (2005), H9; Braunmiller, (unpublished moment tensor), H13; Deichmann et al. (2000), H1–2, H7, H10–12; Deichmann et al. (2002), H18; Deichmann et al. (2004), H19–20, P10; Deichmann et al. (2006), H21; Deichmann et al. (2008), H22; Deichmann et al. (2009), H23; Deichmann et al. (2011), H28; Deichmann et al. (2012), P15; Kastrup et al. (2004), H8; Roth et al. (1992), H3-6, P1–4; Zappone (unpublished), P7, P9

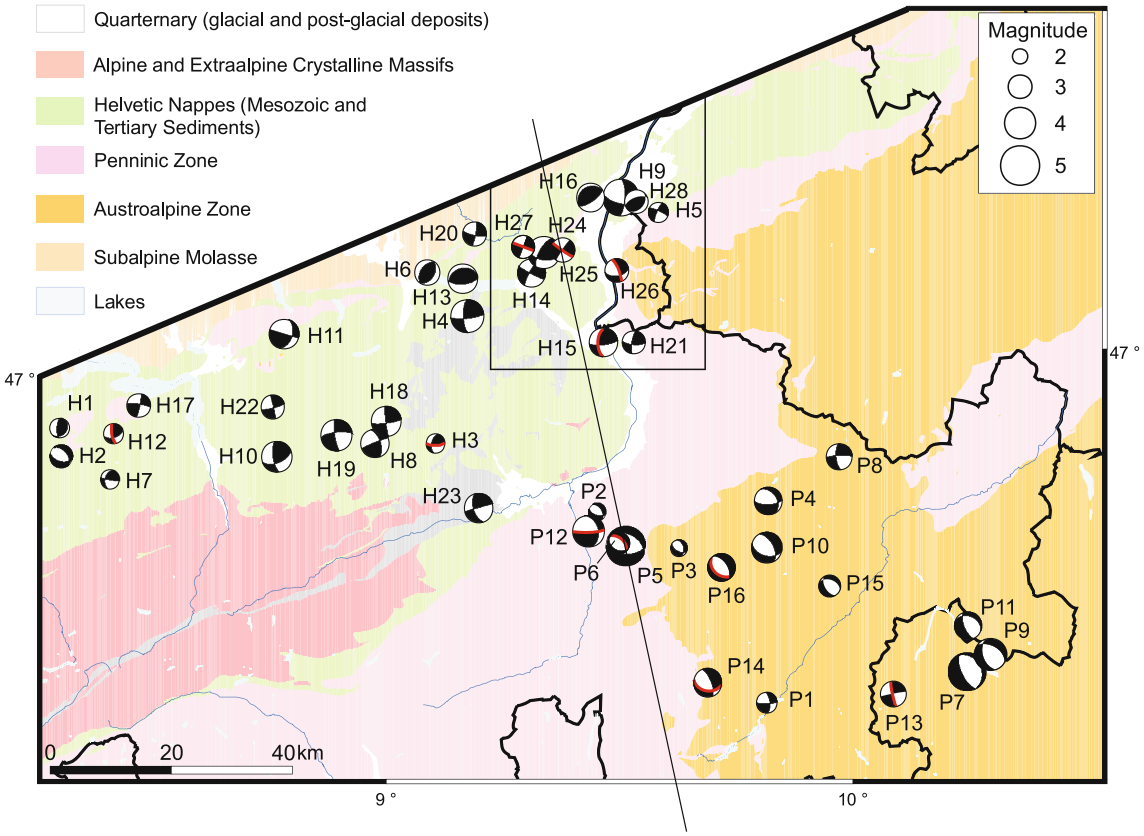

Fig. 4 Tectonic map of the study area (Bundesamt für Wasser und Geologie 2005) with the focal mechanisms (lower-hemisphere equal-area projections) of the events listed in Table 1; the nodal planes which could be identified as the active fault planes are marked in *red*. The *oblique line* is the trace of the cross-section in Fig. 2. The *small polygon* delineates the eastern part of the Helvetic domain discussed in the text, corresponding to the stress-inversion results marked "E-part of Helvetic" in Fig. 6

and the shear stress resolved on all fault planes used in the inversion and is a measure of the degree to which the assumption of a uniform stress field is valid in the given region (e.g. Michael 1991).

5 Discussion

From the stress-inversion analysis, the stress field in the Penninic/Austroalpine domain corresponds to a normal-faulting regime with an almost vertical maximum compressive stress (S1) and a practically horizontal minimum compressive stress (S3) with NE–SW orientation and relatively little scatter (Fig. 6). Whereas the direction of S3 is well constrained by the inversion, the scatter of the possible directions of S1 and S2 forms an almost continuous band along a vertical plane. This is symptomatic for a situation in which the magnitudes of S1 and S2 are similar, a fact that is reflected also in the relatively large Φ value of 0.73 ± 0.08. The average and standard deviation of the

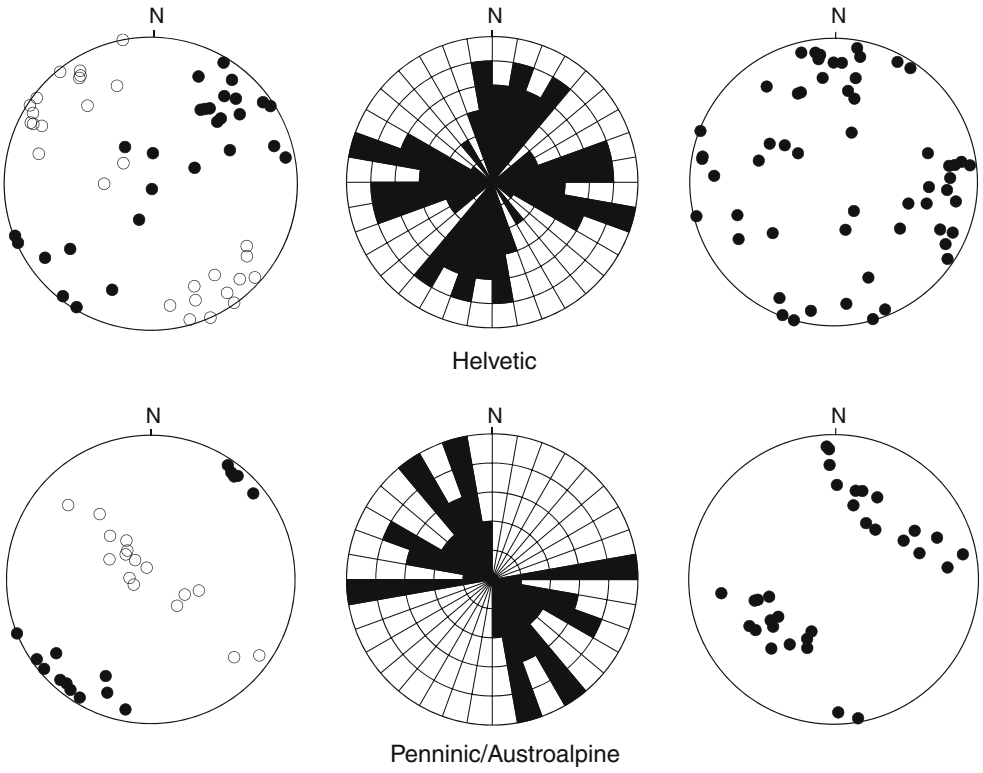

Fig. 5 *Left* stereographic plot (lower-hemisphere, equal area) of azimuth and plunge of the P-axes (*empty circles*) and T-axes (*filled circles*); *middle* symmetric polar histograms showing the azimuthal distribution of the nodal planes; *right* stereographic plot of the normals to all nodal planes. The polar histograms (*rose diagrams*) show the number of nodal planes in azimuth bins of 10°

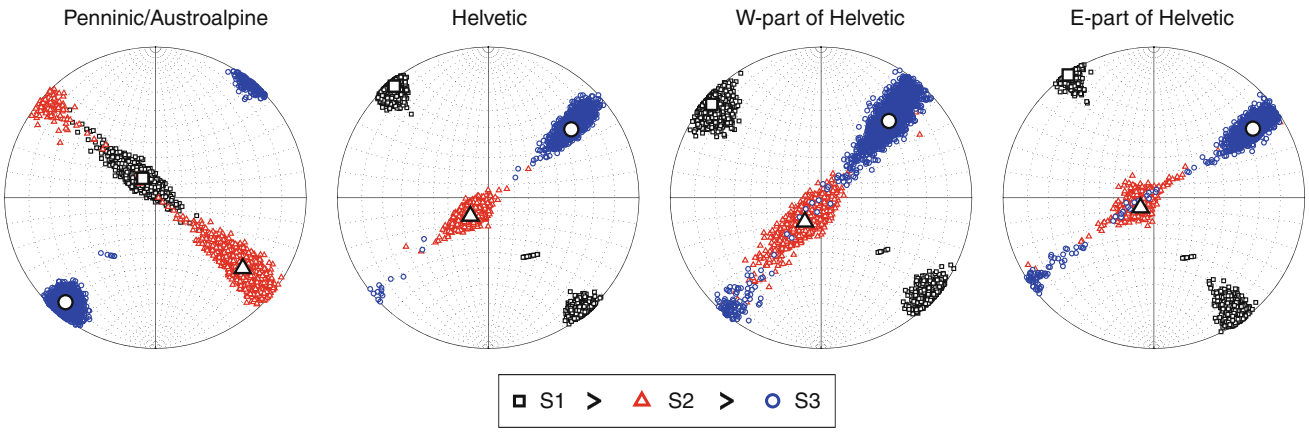

Fig. 6 Results of the stress inversion (lower-hemisphere Wulff-projections) for the Penninic/Austroalpine and the complete Helvetic data sets, as well as for the two Helvetic subsets outlined in Fig. 4. S1, maximum; S2, the intermediate; S3, the minimum compressive stress axis. The *larger white symbols* show the orientation of the principal axes of the optimum stress tensor. The scatter around the optimum orientation for each stress axis shows the 95 % confidence limits of the boot-strap inversions

angle β are small, so that the assumption of a nearly uniform stress field in this region seems to be justified (Michael 1991).

For the Helvetic domain, the stress inversion results in a nearly vertical intermediate stress axis (S2), typical for a strike-slip regime. The S1 axis is practically horizontal and its NW–SE orientation is well constrained and consequently the S3 axis is oriented NE-SW. The Φ value is 0.31 ± 0.08, which implies that the magnitude of S2 is closer to S3 than to S1. This is also reflected in the larger scatter in dip of S2 and S3 than of S1. The average and standard deviation of the angle β is considerably larger for the stress inversion of the Helvetic data set than of the Penninic/Austroalpine data. This might be symptomatic of a non-uniform stress state in the former, a possibility that is also suggested by two cases of thrust and normal faulting events occurring in close proximity to each other (see Fig. 4; Table 1). To test this, we performed the inversion separately for two subsets of the Helvetic data, as outlined in Fig. 4. The selection of the two data subsets was performed by visual inspection of the focal mechanisms, with the goal of maximizing potential differences in stress orientations. Overall, the inversion results of the two data

Table 2 Parameters of the stress inversion results

Tectonic domain	S1 trend/plunge	S2 trend/plunge	S3 trend/plunge	Phi	Beta	Faulting style	Nr. of events
Penninic	327/73	129/17	221/5	0.73 ± 0.08	15 ± 10	Normal	16
Helvetic	320/2	224/71	51/19	0.31 ± 0.08	21 ± 16	Strike slip	28
W-Helvetic	311/3	214/68	42/22	0.28 ± 0.11	24 ± 18	Strike slip	17
E-Helvetic	325/10	233/77	55/13	0.34 ± 0.13	11 ± 8	Strike slip	11

Explanations are given in the text (see chapter 4 and Fig. 6)

subsets are similar to each other and to the data set as a whole: in all three cases we obtain a strike-slip regime with a slight counter-clockwise rotation of the orientation of the principal axes from east to west (Fig. 6). While the average value and standard deviation of β improves for the eastern subset relative to the dataset as a whole, it actually deteriorates slightly for the western subset. Also the scatter of the possible stress orientations increases for the inversions of the subsets, probably due to the fewer data points compared to the entire Helvetic data set. Different ways of subdividing the data set are not likely to change the result significantly. We therefore consider the inversion results based on the Helvetic data set as a whole to be a good representation of the average stress orientation for the given region.

The difference in stress regime between the Helvetic and Penninic/Austroalpine domains is reflected not only in the different orientations of the principle stress axes, but also in their absolute values. Figure 7 is a graphical comparison between the stress levels in the two regions. It is based on three assumptions: (1) one of the principle stress axes is vertical and equal to the lithostatic pressure, (2) the weight of the overburden is the same in both regions, and (3) the friction coefficient and the pore pressure on a given fault are the same in both regions. With these simplifying assumptions and the Φ values obtained from the stress inversion it is possible to compute the stresses required to trigger slip on a fault optimally oriented with respect to each stress field. Figure 7 shows that, at comparable depths below the topographic surface, the differential stress and absolute values of the principle stresses must be greater in the Helvetic than in the Penninic/Austroalpine domain and that as a consequence there must be a horizontal stress gradient across the northern Alpine front. Following Schorlemmer et al. (2005), the higher differential stress necessary to trigger an earthquake under a strike-slip regime compared to a normal faulting environment should manifest itself as differences in the relative frequency of occurrence of larger versus smaller earthquakes. This is quantified by the so-called b-value, which is the slope of the logarithm of the cumulative number of events as a function of their magnitude. As a consequence, we would expect lower b-values, and thus a higher propensity for the occurrence of larger earthquakes, in the Helvetic than in the Penninic/Austroalpine domain.

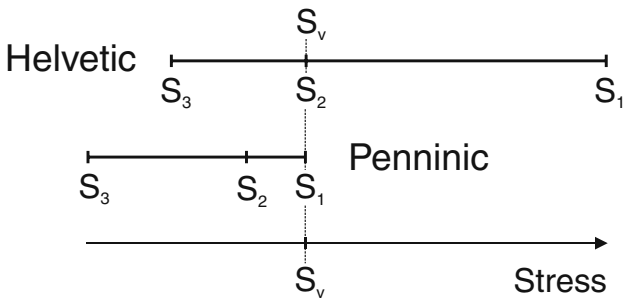

Fig. 7 Diagram illustrating the two stress regimes in relation to the vertical stress (Sv). Stress magnitudes increase from *left* to *right*. For each region, the value of the intermediate principal stress (S2) relative to the maximum (S1) and to minimum principal stress (S3) is based on the computed Φ values. Sv is assumed to be equal for both regions. In the Helvetic domain Sv = S2 (strike-slip regime) while in the Penninic domain Sv = S1 (normal-faulting regime). The length of each *horizontal bar* is proportional to the differential stress needed to trigger an earthquake on an optimally oriented fault under the two stress regimes. It follows that both differential and absolute stresses are higher in the Helvetic than in the Penninic/Austroalpine domain

Whether this is the case and the data is sufficient to resolve such a difference will be examined in the course of an ongoing reassessment of the seismic hazard in Switzerland.

It is remarkable that most of the normal faulting events are located in the Penninic nappes, units that were emplaced during the Alpine orogeny as a consequence of large-scale and long-lasting thrusting and crustal shortening. Thus tectonic units that were formed under compression are now deforming under extension. This is illustrated in the depth cross-section shown in Fig. 2 for a subset of the available focal mechanisms, e.g. the events of Vaz, Feldis, Lenzerheide and Bivio. It is likely that also the normal-faulting events of Sertig and Filisur, located east of this cross-section, occurred in the Penninic nappes underlying the Austroalpine units visible at the surface. Thus the situation is practically identical to that observed in the Valais (e.g. Maurer et al. 1997), where the normal-faulting events are concentrated in the stack of nappes above the Penninic thrust.

An explanation for the differences in faulting style and stress regimes between the Helvetic and Penninic/Austroalpine domains can be found from a comparison with the crustal uplift rates. Uplift rates of 1.2–1.6 mm/year observed in the Penninic/Austroalpine domain of

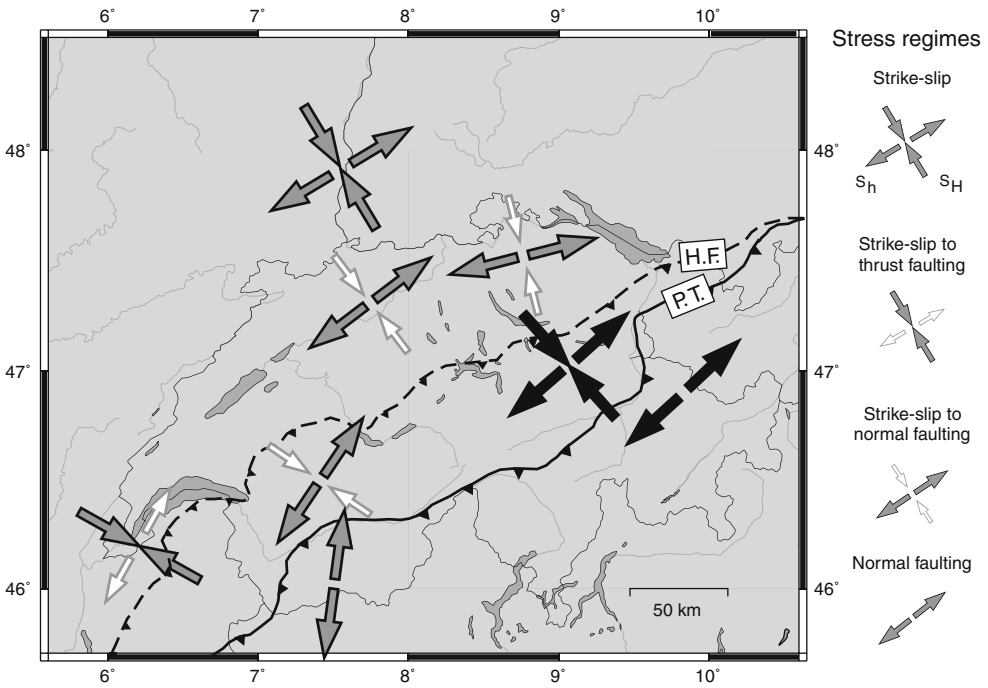

Fig. 8 Stress regimes in Switzerland (modified after Kastrup et al. 2004), *grey arrows* stress orientations determined by Kastrup et al. (2004), *black arrows* new or updated stress orientations (this study)

Graubünden are among the highest in all of Switzerland (e.g. Schlatter and Marti 2002). Towards the north, uplift rates decrease rapidly and in the area of the northern Helvetic front they amount to only a few tenths of a mm/yr. In fact, a map reproduced in Kahle et al. (1997) shows that the Helvetic domain in the northern Valais and north of Graubünden with the predominance of strike-slip events are the regions with the strongest uplift rate gradients in Switzerland. This fact is also visualized by Persaud and Pfiffner (2004) in a plot of uplift rates along a profile parallel to the cross-section in our Fig. 2. Although it is not possible to establish a more detailed correlation between, for example, the orientation of the T-axes of the focal mechanisms and the trend of the uplift rate gradient, the correlation of the variation of stress regimes demonstrated by the earthquake focal mechanisms and the change in uplift rates is significant (e.g. Sue et al. 2007).

The resulting extensional regime in regions of a topographic high, large crustal thickness and strong uplift is similar to what was found in the Western Alps by Sue et al. (1999) and Delacou et al. (2004) and in the Valais by Maurer et al. (1997) and Kastrup et al. (2004). Figure 8 places our results into a regional context. As discussed by Kastrup et al. (2004), the stress field in the northern Alpine foreland is the consequence of the opening of the Atlantic Ocean and the slow but ongoing convergence between Africa and Europe. This they consider to represent the regional stress field. Based on the assumption that the orientation of S3 in the Penninic/Austroalpine domain of Graubünden is equal to the mean trend of the T-axes of the focal mechanisms available to them at that time, Kastrup et al. (2004) postulated a counter-clock rotation of 49° of S3 in Graubünden relative to this regional stress field. They explained this rotation as the consequence of the superposition of the regional stress field and a uniaxial extensional stress oriented perpendicularly to the strike of the orogen. Such extensional stresses in the highest regions of a mountain belt are expected as a consequence of the topography and of the lateral density variations due to the crustal root below the orogen (see Sue et al. 2007 and references therein). The lateral density variations below the Alps are documented, for instance, in Kissling et al. (2006). According to the analysis of Kastrup et al. (2004), based on the observed stress rotation and the local strike of the orogen, the magnitudes of the regional differential stress and the local uniaxial stress must be nearly equal, and Sue et al. (2007) speak of a *"subtle balance between boundary forces and buoyancy forces"*. Our results indicate that the rotation of S3 between the foreland and the orogen is only about 39°. However, considering the scatter of the stress orientations obtained from the inversions, which is on the order of 10°, the difference between 39° and 49° of the rotation angle is not significant, and an update of the analysis performed by Kastrup et al. (2004) based on the smaller rotation angle obtained from our stress inversion will not change their conclusion substantially.

6 Conclusions

As has been observed in the Western Alps (e.g. Delacou et al. 2004; Sue et al. 2007) and in the Penninic domain of

the southern Valais (e.g. Maurer et al. 1997), the stress field in the Penninic/Austroalpine domain of the eastern Swiss Alps is characterized by extension oriented at a high angle relative to the strike of the orogen. Thus, the Penninic nappes, which were emplaced as large-scale compressional structures during the Alpine orogenesis, are now deforming in an extensional mode. This contrasts with the more compressional strike-slip regime in the Helvetic domain of the northern Alpine front. Whereas the Penninic/Austroalpine domain is an area with some of the highest uplift rates in all of Switzerland, the Helvetic domain is characterized by the strongest uplift rate gradient.

Relative to the northern Alpine foreland, the orientation of the least compressive stress in the Penninic/Austroalpine domain is rotated counter-clockwise by about 40°. It is generally accepted (e.g. Kastrup et al. 2004) that the stress observed in the northern Alpine foreland reflects the regional stress field, which is due to the opening of the Atlantic and the ongoing convergence between the African and European continental plates. Following Kastrup et al. (2004), the observed rotation of the orientation of the least compressive stress in the Penninic/Austroalpine region can be explained as the superposition of this regional stress field and a uniaxial extensional stress perpendicular to the local trend of the Alpine mountain belt. As discussed in detail by Sue et al. (2007), such a spreading stress in regions of elevated topography and large uplift rates is expected from lateral density variations due to a crustal root.

Acknowledgments This research was partially funded by the Swiss National Science Foundation under the Marie Heim-Vögtlin Program. We thank Jan Pleuger and an anonymous reviewer for their thorough and constructive reviews, and Sabine Wöhlbier for help with the seismotectonic map.

References

Aki, K., & Richards, P. G. (1980). *Quantitative seismology—theory and methods* (Vol. 1). San Francisco: Freeman.

Baer, M., Deichmann, N., Ballarin Dolfin, D., Bay, F., Delouis, B., Fäh, D., et al. (1999). Earthquakes in Switzerland and surrounding regions during 1998. *Eclogae Geologicae Helvetiae, 92*(2), 265–273.

Baer, M., Deichmann, N., Braunmiller, J., Ballarin Dolfin, D., Bay, F., Bernardi, F., et al. (2001). Earthquakes in Switzerland and surrounding regions during 2000. *Eclogae Geologicae Helvetiae, 94*(2), 253–264.

Baer, M., Deichmann, N., Braunmiller, J., Clinton, J., Husen, S., Fäh, D., et al. (2007). Earthquakes in Switzerland and surrounding regions during 2006. *Swiss Journal of Geosciences, 100*(3), 517–528. doi:10.1007/s00015-007-1242-0.

Bernardi, F., Braunmiller, J., & Giardini, D. (2005). Seismic moment from regional surface-wave amplitudes: applications to digital and analog seismograms. *Bulletin of the Seismological Society of America, 95*(2), 408–418. doi:10.1785/0120040048.

Braunmiller, J., Kradolfer, U., Baer, M., & Giardini, D. (2002). Regional moment tensor determination in the European–Mediterranean area—initial results. *Tectonophysics, 356*, 5–22.

Bundesamt für Wasser und Geologie. (2005). *Tektonische Karte der Schweiz 1:500,000*. Bern: Geologische Bearbeitung durch Institut für Geologie, Universität Bern. ISBN 3-906723-56-9.

Deichmann, N., Baer, M., Braunmiller, J., Ballarin Dolfin, D., Bay, F., Bernardi, F., et al. (2002). Earthquakes in Switzerland and surrounding regions during 2001. *Eclogae Geologicae Helvetiae-Swiss Journal of Geosciences, 95*(2), 249–261.

Deichmann, N., Baer, M., Braunmiller, J., Cornou, C., Fäh, D., Giardini, D., et al. (2004). Earthquakes in Switzerland and surrounding regions during 2003. *Eclogae Geologicae Helvetiae-Swiss Journal of Geosciences, 97*(3), 447–458.

Deichmann, N., Baer, M., Braunmiller, J., Husen, S., Fäh, D., Giardini, D., et al. (2006). Earthquakes in Switzerland and surrounding regions during 2005. *Eclogae Geologicae Helvetiae-Swiss Journal of Geosciences, 99*(3), 443–452. doi:10.1007/s00015-006-1201-1.

Deichmann, N., Baer, M., Clinton, J., Husen, S., Fäh, D., Giardini, D., et al. (2008). Earthquakes in Switzerland and surrounding regions during 2007. *Swiss Journal of Geosciences, 101*(3), 659–667. doi:10.1007/s00015-008-1304-y.

Deichmann, N., Ballarin Dolfin, D., Kastrup, U. 2000. *Seismizitaet der Nord- und Zentralschweiz.* Nagra Technischer Bericht, NTB 00-05, Nagra, Wettingen.

Deichmann, N., Clinton, J., Husen, S., Edwards, B., Haslinger, F., Fäh, D., et al. (2011). Earthquakes in Switzerland and surrounding regions during 2010. *Swiss Journal of Geosciences, 104*(3), 537–547. doi:10.1007/s00015-011-0084-y.

Deichmann, N., Clinton, J., Husen, S., Edwards, B., Haslinger, F., Fäh, D., Giardini, D., Kästli, P., Kradolfer, U., Wiemer, S. (2012). Earthquakes in Switzerland and surrounding regions during 2011. Swiss Journal of Geosciences, 105(3). doi:10.1007/s00015-012-0116-2.

Deichmann, N., Clinton, J., Husen, S., Haslinger, F., Fäh, D., Giardini, D., et al. (2009). Earthquakes in Switzerland and surrounding regions during 2008. *Swiss Journal of Geosciences, 102*(3), 505–514. doi:10.1007/s00015-009-1339-8.

Delacou, B., Sue, C., Champagnac, J.-D., & Burkhard, M. (2004). Present-day geodynamics in the bend of the western and central Alps as constrained by earthquake analysis. *Geophysical Journal International, 158*, 753–774.

Eva, E., Pastore, S., & Deichmann, N. (1998). Evidence for ongoing extensional deformation in the western Swiss Alps and thrust-faulting in the southwestern Alpine foreland. *Journal of Geodynamics, 26*(1), 27–43.

Eva, E., & Solarino, S. (1998). Variations of stress directions in the western Alpine arc. *Geophysical Journal International, 135*, 438–448.

Eva, E., Solarino, S., & Eva, C. (1997). Stress tensor orientation derived from fault plane solutions in the southwestern Alps. *Journal of Geophysical Research, 102*, 8171–8185.

Kahle, H.-G., Geiger, A., Bürki, B. Gubler, E., Marti, U., Wirth, B., Rothacher, M., Gurtnar, W., Beutler, G., Bauersima, I., Pfiffner, A.O. 1997. Recent crustal movements, geoid and density distribution: contribution from integrated satellite and terrestrial measurements. In O. A. Pfiffner et al. (Eds.), *Deep structure of the Alps, results of NRP20*, (pp. 251–259). Basel: Birkhäuser.

Kastrup, U. 2002. Seismotectonics and stress field variations in Switzerland. Ph.D. Thesis Nr. 14527, ETH-Zurich.

Kastrup, U., Zoback M.-L., Deichmann, N., Evans, K., Giardini, D., Michael, A.J. 2004. Stress field variations in the Swiss Alps and the northern Alpine foreland derived from inversion of fault plane solutions. *Journal of Geophysical Research, 109*(B1). doi:10.1029/2003JB002550B01402.

Kissling, E., Schmid, S.M., Lippitsch, R., Ansorge, J., Fügenschuh, B. 2006. Lithosphere structure and tectonic evolution of the Alpine arc: new evidence from high-resolution teleseismic tomography.

In D. G. Gee, R. A. Stephenson (Eds.), *European lithosphere dynamics*. Geological Society, London, Memoirs, *32*, 129–145.

Maurer, H., Burkhard, M., Deichmann, N., & Green, A. G. (1997). Active tectonism in the western Swiss Alps. *Terra Nova, 9*, 91–94.

Michael, A. J. (1984). Determination of stress from slip data: faults and folds. *Journal of Geophysical Research, 89*, 11517–11526.

Michael, A. J. (1987a). The use of focal mechanisms to determine stress; a control study. *Journal of Geophysical Research, 92*, 357–368.

Michael, A. J. (1987b). Stress rotation during the Coalinga aftershock sequence. *Journal of Geophysical Research, 92*, 7963–7979.

Michael, A. J. (1991). Spatial variations in stress within the 1987 Whittier Narrows, California, aftershock sequence: new techniques and results. *Journal of Geophysical Research, 96*, 6303–6319. doi:10.1029/91JB00195.

Nagra (2008). Vorschlag geologischer Standortgebiete für das SMA- und HAA-Lager—Geologische Grundlagen. Technischer Bericht NTB 08-04, Beilage 2.2-2.

Pavoni, N., Maurer, H., Roth, P., Deichmann, N. 1997. Seismicity and seismotectonics of the Swiss Alps. In O. A. Pfiffner et al. (Eds,), *Deep structure of the Alps, results of NRP20*, (pp. 241–250). Basel: Birkhäuser.

Pavoni, N., & Mayer-Rosa, D. (1978). Seismotektonische Karte der Schweiz, 1:750,000. *Eclogae Geologicae Helvetiae, 71*, 293–295.

Persaud, M., & Pfiffner, O. A. (2004). Active deformation in the eastern Swiss Alps: post-glacial faults, seismicity and surface uplift. *Tectonophysics, 385*, 59–84.

Pfiffner, O.A. & Hitz, L. (1997). Geologic interpretation of the seismic profiles of the Eastern Traverse (lines E1–E3, E7–E9): eastern Swiss Alps. In O. A. Pfiffner et al. (Eds.), *Deep structure of the Alps, results of NRP20* (pp. 73–100). Basel: Birkhäuser.

Pfiffner, O.A., Kühni, A., Jemelin, L. (1997). Geologische und hydrologische Profile, Teil 1: Geologie. In: *Hydrologischer Atlas der Schweiz, Tafel 8.2*, Landeshydrologie, Bern.

Roth, P., Pavoni, N., & Deichmann, N. (1992). Seismotectonics of the Swiss Alps and evidence for precipitation-induced variations of seismic activity. *Tectonophysics, 207*, 183–197.

Schlatter, A., & Marti, U. (2002). Neues Landeshöhennetz der Schweiz LHN95. *Mensuration, Photogrammétrie, Génie Rural, 1*, 13–17.

Schmid, S.M., Pfiffner, O.A., Schreurs, G. (1997). Rifting and collision in the Penninic Zone of eastern Switzerland. In O. A. Pfiffner et al. (Eds.), *Deep structure of the Alps, results of NRP20* (pp. 160–185). Basel: Birkhäuser.

Schorlemmer, D., Wiemer, S., & Wyss, M. (2005). Variations in earthquake-size distribution across different stress regimes. *Nature, 437*, 539–542.

Sue, C., Delacou, B., Champagnac, J. D., Allanic, C., Tricart, P., & Burkhard, M. (2007). Extensional neotectonics around the bend of the Western/Central Alps: an overview. *International Journal of Earth Sciences, 96*, 1101–1129.

Sue, C., Thouvenot, F., Fréchet, J., & Trichart, P. (1999). Widespread extension in the core of the western Alps revealed by earthquake analysis. *Journal of Geophysical Research, 104*, 25611–25622.

Zoback, M.-L. 1992. First- and second-order patterns of stress in the lithosphere: The World Stress Map Project. *Journal of Geophysical Research, 97*(B8), 11703–11711.